Poly-L-lysine Glycoconjugates Inhibit DC-SIGN-mediated Attachment of Pandemic Viruses

Jonathan Cramer,[1),‡] Butrint Aliu,[1),‡] Xiaohua Jiang,[1)] Timothy Sharpe,[2)] Lijuan Pang,[1)] Adrian Hadorn,[1)] Said Rabbani,[1)] and Beat Ernst[1)*]

[1)] University of Basel, Department of Pharmaceutical Sciences, Pharmacenter of the University of Basel, Klingelbergstrasse 50, 4056, Basel, Switzerland

[2)] University of Basel, Biophysics Facility, Biocenter of the University of Basel, Klingelbergstrasse 70, 4056, Basel, Switzerland

* Corresponding author. Tel.: +41 61 207 15 51; Fax: +41 61 207 15 52; E-mail: beat.ernst@unibas.ch (B. Ernst)

‡ These authors contributed equally.

***Keywords**:* C-type lectin receptors, COVID-19, SARS-CoV-2, Ebola, HIV, poly-L-lysine, multivalency, thermodynamics.

***Abbreviations**:* CRD, carbohydrate recognition domain; ITC, isothermal titration calorimetry; K_D, dissociation constant; DC-SIGN, dendritic cell-specific intercellular adhesion molecule 3 grabbing non-integrin; PLL, poly-L-lysine; DLS, dynamic light scattering; AUC, analytical ultracentrifugation; MeMan, methyl α-D-mannoside.

Abstract (229 words)

Envelope glycoproteins of many viruses are heavily glycosylated. Among other functions, virus glycans can mediate interactions with host receptors and contribute to internalization and virus dissemination. The C-type lectin receptor DC-SIGN, which is expressed by cells of the innate immune system, can act as an entry receptor for pathogens, including pandemic viruses such as SARS-CoV-2, ebola, and HIV. In the context of the recent SARS-CoV-2 pandemic, this mechanism has been linked to severe cases of COVID-19. Inhibition of the interaction between DC-SIGN and viral envelope glycoproteins has therefore the potential to generate broad spectrum antivirulent agents. Moreover, the important role of this mechanism in numerous viral infections, as well as an interaction partner conserved in the host genome highlight the potential of DC-SIGN-targeted therapeutics not only for the treatment of existing infections, but also for the rapid response to future pandemics with newly emerging virus serotypes. Here, we demonstrate that mannose-functionalized poly-L-lysine glycoconjugates efficiently inhibit the attachment of viral glycoproteins from SARS-CoV-2, ebola, and HIV to DC-SIGN-presenting cells with up to picomolar affinity. Treatment of susceptible cells leads to prolonged receptor internalization and statistically significant inhibition of virus binding for up to 6 h. Furthermore, the polymers are fully biocompatible and readily cleared by the target cells. Finally, the thermodynamic analysis of these multivalent interactions revealed an entropy-driven affinity enhancement, opening promising perspectives for the future development of multivalent therapeutics.

Introduction

Envelope glycoproteins of a variety of viruses are densely covered with host-derived carbohydrates. These glycan structures shield viruses from antibody-mediated immune responses, enabling the attachment to the host's lectins [1,2] One of these lectins is the C-type lectin receptor (CLR) DC-SIGN (dendritic cell-specific intercellular adhesion molecule 3 grabbing non-integrin), a surface receptor expressed by innate immune cells. It has been demonstrated that DC-SIGN acts as an entry receptor for pathogens and plays a detrimental role in the pathology of many viral infections by promoting virus dissemination and immune evasion.[1–4] High-mannose glycan epitopes on envelope glycoproteins of epidemic and pandemic viruses such as HIV,[5] ebola,[6,7] influenza A,[8] hepatitis C,[9] SARS,[10] zika,[11] dengue,[12] and others,[1] have been shown to enable DC-SIGN mediated attachment and internalization, either for *cis*-infection of myeloid cells or for *trans*-infection of other cell types.[4,10,13,14]

In the context of the ongoing SARS-CoV-2 pandemic, increasing evidence points to a possible involvement of DC-SIGN in virus attachment to innate immune cells.[15] The SARS-CoV-2 spike protein is heavily glycosylated with high mannose and complex N-glycans, which potentially could serve the attachment to host lectins.[16] In fact, several groups have demonstrated that these glycans are indeed recognized with picomolar affinity by various CLRs such as DC-SIGN and the closely related DC-SIGNR.[17–21] The interaction of the viral spike glycoprotein leads to internalization in DC-SIGN-presenting cells, strongly implicating DC-SIGN as an ACE2-independent entry receptor for SARS-CoV-2. Infection of innate immune cells by this mechanism could contribute to the exaggerated immune response in severe COVID-19. This is consistent with the fact that DC-SIGN expression levels were increased in severe COVID-19 patients with elevated amounts of proinflammatory monocyte-derived macrophages, inflammatory cytokines and chemokines.[17] Another recent study confirmed DC-

SIGN-mediated internalization of SARS-CoV-2 pseudovirions into monocyte-derived dendritic cells, albeit without *cis*-infection of the cells.[22] However, dendritic cells pre-treated with SARS-CoV-2 pseudovirions efficiently infected $ACE2^+$ Vero cells in a *trans*-infection assay, thereby indicating a deciding role of DC-SIGN for virus dissemination from the lung to other tissues. Importantly, *trans*-infection could be inhibited with a known DC-SIGN ligand. Differences in SARS-CoV-2 virulence due to mutation in the viral spike glycoprotein, such as the prominent D614G mutation, have been attributed to potential variations in glycosylation, resulting in differences in the interaction with DC-SIGN and DC-SIGNR.[15] Furthermore, a recent study concluded that genetic variants in the *ABO* gene locus correlate with DC-SIGN expression levels and that increased DC-SIGN expression represents a genetic risk factor for severe COVID-19, indicating a central role of the innate immune system in this disease.[23]

With this background, inhibition of DC-SIGN-mediated attachment of viral particles to innate immune cells represents a promising strategy for the development of antiviral drugs.[24–26] In the past, this strategy has been investigated for the treatment of HIV,[20] ebola,[27] zika,[28] and dengue infections.[28] In view of the recent emergence of the SARS-CoV-2 pandemic, DC-SIGN-targeted antivirals could represent a promising host-directed treatment option for COVID-19. Importantly, metabolic pathways responsible for glycosylation of viral proteins, as well as the targeted glycan receptors are evolutionarily conserved in the host genome. It can therefore be assumed, that the pharmacological interference in this mechanism with antiviral therapeutics is insensitive to viral resistance mutations and additionally provides the possibility for an early containment of infections from newly emerging virus strains with pandemic potential.[29]

Multivalent presentations of viral glycans employing mannose or fucose epitopes have been explored as potential inhibitors of DC-SIGN-mediated virus attachment. Multivalent carbohydrate-lectin interactions often proceed via statistical rebinding, or a bind-and-jump

mechanism.[30,31] Accordingly, carbohydrate epitopes on a multivalent scaffold migrate along a surface presenting the carbohydrate recognition domain (CRD) of the lectin, while undergoing numerous association and dissociation events. Even though the individual monovalent interactions of the epitopes are weak, the macroscopic apparent binding affinity, i.e. the probability of the lectin being bound to any carbohydrate ligand on the surface, is much higher. This mechanism leads to an increase in apparent binding affinity of protein-carbohydrate interactions of up to a factor of 10^6.[32,33] In this context, functionalized polymeric supports,[34] peptides,[35] dendrimers,[36] nanoparticles,[37] fullerenes,[28] carbon nanotubes,[27] and thiacalixarenes[38] have been studied. However, a severe drawback of some of these non-biodegradable multivalent scaffolds is their potential accumulation and associated toxicity, especially when prolonged pulmonary applications are considered.[39,40]

Here, we report the synthesis and biological evaluation of mannosylated poly-L-lysine glycoconjugates (Man-PLL) **1a-d** as multivalent ligands for DC-SIGN. By relying on poly-L-lysine as a polymeric scaffold we resort to a broadly available system that is easily modified, non-immunogenic, biodegradable, and extensively studied for biological applications.[41–44] We demonstrate that glycopolymers **1a-d** efficiently block the interaction of DC-SIGN expressing (DC-SIGN$^+$) cells with viral glycoproteins from HIV, Ebola, and SARS-CoV-2. In addition, we show that the glycopolymers are readily cleared by the target cells and, thus, show great potential for compatibility with prolonged pulmonary application in a therapeutic setting. In addition, the binding affinity, thermodynamics, and stoichiometry of the multivalent interactions between glycopolymers **1a-d** and recombinant DC-SIGN are characterized by isothermal titration calorimetry (ITC).

Results and Discussion

Man-PLL **1a-d** were synthesized from commercially available poly-L-lysine hydrobromide (**2**) by chloroacetylation (→ **3**) followed by chloride substitution with various amounts of the thiol functionalized mannoside (**4**) (Scheme 1).[45] The unreacted chloroacetamides were then reacted with an excess of thioglycerol. This operationally simple synthetic sequence yielded the water-soluble glycopolymers **1a-d** with varying carbohydrate loadings. It is important to note that commercially available poly-L-lysine polymers are polydisperse systems with a degree of polymerization distributed around a statistical mean. This affects all calculations of concentration, loading, and affinity, which represent estimates based on the assumption of an ideal, monodisperse polymer.

Synthesis of Man-PLL 1a-d

Mannose building block **4** was obtained in an overall yield of 25 % in a short synthetic sequence starting from D-mannose pentaacetate (**5**). α-Selective glycosylation with 3-chlorpropan-1-ol yielded mannoside **6**. Azide substitution of chloride (→ **7**), Zemplén deacetylation (→ **8**) and catalytic hydrogenation gave the unprotected amine **9**. Finally, reaction with γ-thiobutyrolactone gave building block **4** in good yield.

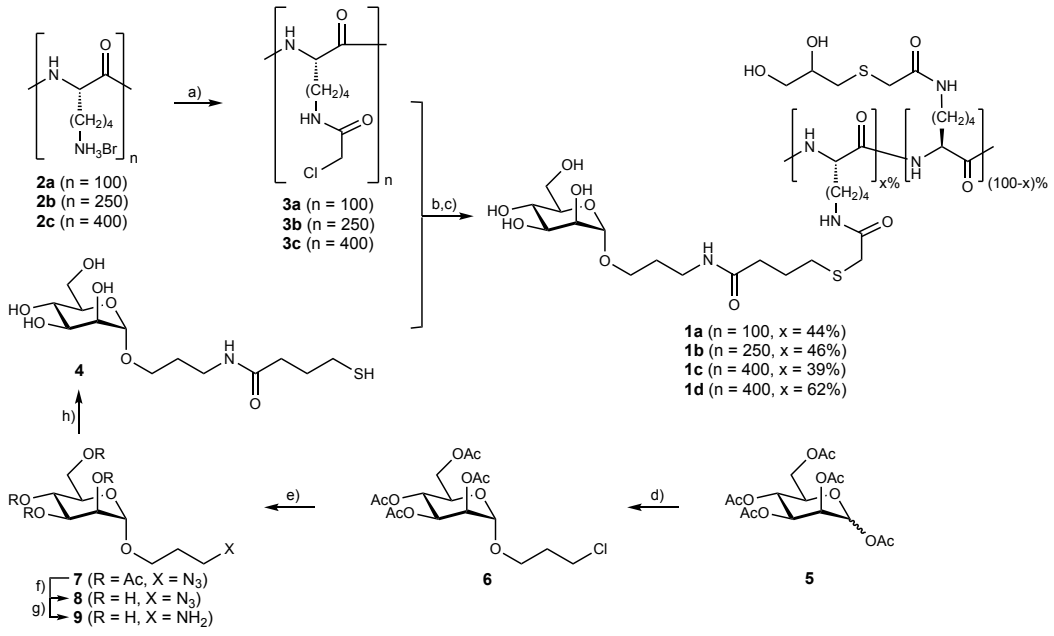

Scheme 1. Synthesis of the mannosylated poly-L-lysine glycoconjugates **1a-d;** (a) 2,6-lutidine, chloroacetic anhydride, 4°C, 16h (**3a** (92%), **3b** (62%), **3c** (96%)); b) 1,8-diazabicyclo(5.4.0)undec-7-ene/DMF, building block **4**, without purification c) thioglycerol, Et_3N, shaken overnight: **1a** (45%, loading 44%); **1b** (64%, loading 46%); **1c** (68%, loading 39%); **1d** (51%, loading 62%). d) 3-chloro-1-propanol, $BF_3 \bullet Et_2O/CH_2Cl_2$, rt, overnight, (65%); (e) NaN_3/DMF, 60°C, 2h, (95%); (g) MeONa/MeOH, rt, overnight, (83%); (h) $Pd(OH)_2$/C in MeOH, H_2, (84%); (i) γ-thiobutyrolactone, MeOH/Et_3N, rt, overnight, (68%).

According to this strategy, a series of Man-PLL of different lengths and loadings were prepared (Table 1).

Table 1. Poly-L-lysine glycopolymers prepared for the study of DC-SIGN binding.

Compound	Degree of polymerization; lysine residues n	Absolute number of mannose residues by NMR	Carbohydrate loading x	Average molecular weight [kDa]
Man-PLL$_{100}$ (1a)	100	44	44%	37.8
Man-PLL$_{250}$ (1b)	250	115	46%	95.0
Man-PLL$_{400}$ (1c)	400	156	39%	146.6
Man-PLL$_{400}$ (1d)	400	248	62%	167.9

Biophysical characterization of Man-PLL polymers

The size distribution and the shape of Man-PLL **1a-d** in solution were elucidated by dynamic light scattering (DLS) experiments and analytical ultracentrifugation (AUC). As shown in Table 2, Figure 1A, the measured hydrodynamic diameters (D_h) of **1a-d** reflect the degree of polymerization. A D_h of 9.2 nm was found for Man-PLL$_{100}$ (**1a)**, which is roughly doubled for the 250-mer **1b** (19.8 nm) and tripled for the larger 400-mers **1c** and **1d** (30 nm). The polydispersity indices (Đ) fall in a range of 0.3 to 0.4, indicating the presence of multiple species in the polymer samples, as expected for the polydisperse PLL scaffolds. Next, diffusion-deconvoluted differential sedimentation coefficient distributions (c(s) distributions) were determined by analytical ultracentrifugation (AUC) and signal-weight average sedimentation coefficients (S) were calculated for each polymer (Table 2, Figure 1B). Values of frictional

ratio (f/f_0) fitted from AUC data provide information about the shape of macromolecules in solution. Whereas a value for f/f_0 of 1 corresponds to a spherical shape, values >2.0 indicate a highly extended conformation. Based on sedimentation velocity data, a narrow distribution with an average sedimentation coefficient of 2.21 S was obtained for Man-PLL$_{100}$ (**1a**). These parameters were used to calculate a molecular mass estimate of 39.6 kDa, which correlates well with the theoretical value of 37.8 kDa. For Man-PLL$_{100}$ (**1a**), the recorded frictional ratio of 1.4 suggests a globular shape, comparable to a folded protein. The hydrodynamic radius (D_h) calculated from the average sedimentation coefficient is 6.6 nm. Experimental data for the larger glycopolymers **1b-d** showed more complex distributions, revealing the presence of multiple species with sedimentation coefficients between 2 and 15 S. Molecular mass estimations for these species correlate not only to polymer monomers, but also dimers and higher order aggregates (Figure S10). The calculated D_h from the average sedimentation coefficients are between 20.9 nm and 24.3 nm, a sign for larger particle sizes for the longer polymers compared with **1a**, which corroborates DLS data. Finally, based on the average frictional ratios with values between 2.37 and 2.52, a highly extended conformation of the polymers can be assumed.

Table 2. Biophysical characterization of Man-PLL **1a-d** by DLS and AUC.

Man-PLL	DLS		AUC		
	D_h [nm][a,b]	Đ	Sedimentation coefficient [S][c]	f/f_0	D_h [nm]
1a	9.2 ± 0.4	0.4 ± 0.01	2.21	1.41	6.6
1b	19.8 ± 0.3	0.4 ± 0.05	4.04	2.50	20.9
1c	32.0 ± 0.4	0.3 ± 0.02	5.08	2.37	21.5
1d	27.2 ± 0.7	0.4 ± 0.02	5.24	2.52	24.3

[a] Z-Average values are reported as hydrodynamic radii. [b] The standard deviation from three independent experiments is given as an estimation of experimental error. [c] Signal weighted average over the range 1-20 S. D_h, hydrodynamic diameter; Đ, polydispersity index; f/f_0, frictional ratio.

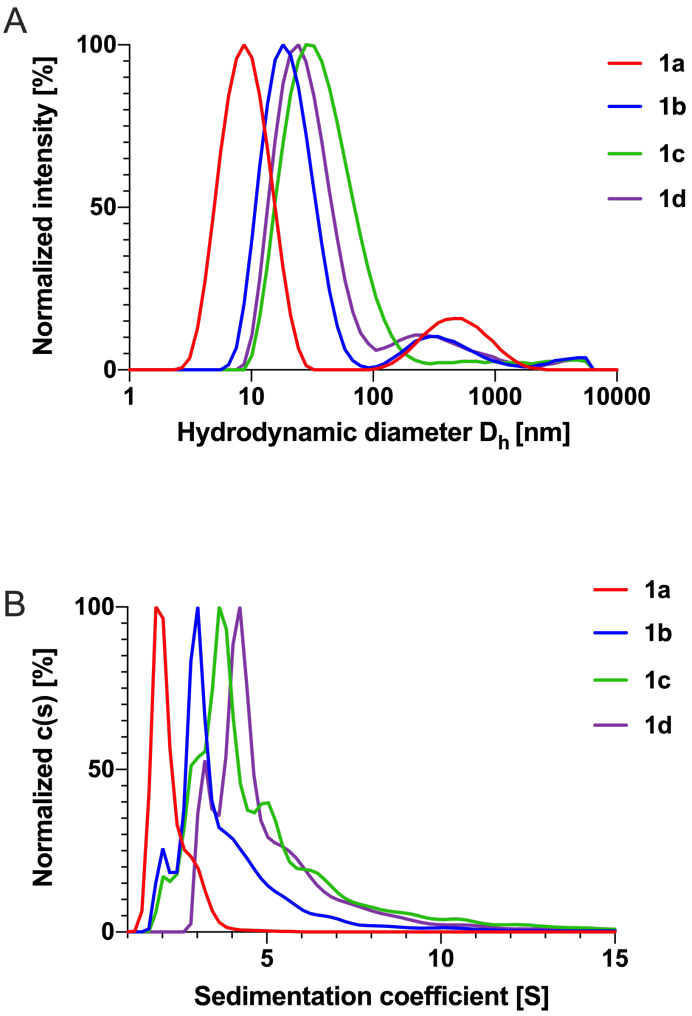

Figure 1. A) Normalized scattering intensity distribution for Man-PLL **1a**-**d** as determined by DLS. B) Normalized diffusion-deconvoluted differential sedimentation coefficient distributions (c(s) distributions) for **1a**-**d** determined by sedimentation velocity AUC experiments. The magnitude of c(s) at a given S value gives the proportion of the total material in that sample having that S value.

Competitive inhibition of viral glycoprotein binding to DC-SIGN$^+$ cells

The potential of Man-PLL **1a-d** to inhibit the attachment of viral glycoproteins from SARS-CoV-2 (spike glycoprotein S1 subunit), ebola (EBOV glycoprotein), or HIV (gp120 envelope glycoprotein) to DC-SIGN$^+$ B-THP-1 cells was investigated using a flow-cytometric assay (Figure 2). DC-SIGN$^+$ cells or isotype controls were incubated with the viral glycoproteins labeled with the cyanine dye Cy5 in the presence of either logarithmic dilutions of

glycopolymers **1a**-**d** or buffer, as described in the experimental section. The amount of fluorescently labeled glycoprotein bound to the cell surface was determined by mean fluorescence intensity and the resulting competition curves were fitted to a four parameter Hill model to determine IC_{50} values. The shortest Man-PLL_{100} (**1a**) showed an IC_{50} value of 43 nM for SARS-CoV-2 spike S1 and 36 nM for EBOV glycoprotein. In contrast, the affinities for the intermediate length Man-PLL_{250} (**1b**) are in the subnanomolar range (789 pM and 637 pM), which corresponds to an affinity gain of approximately a factor of 50. However, further elongation of the polymer backbone (**1b** → **1c**) and increase in mannose loading (**1c** → **1d**) resulted only in a moderate increase of the binding affinities by a factor of two. With IC_{50} values around 200 pM, **1d** is a highly potent inhibitor of the interaction between SARS-CoV-2 spike S1 and EBOV glycoprotein with DC-SIGN. Compared with the monovalent epitope methyl α-D-mannoside (MeMan, IC_{50} = 6.5 mM), the multivalent affinity enhancement is in the order of 10^7. For HIV gp120, an identical trend in affinity was observed, however with absolute IC_{50} values being worse by a factor of five. For the most potent Man-PLL_{400} (**1d**), this resulted in an IC_{50} value of 1.0 nM. The less potent inhibition of the gp120/DC-SIGN interaction is probably linked to a higher binding affinity of the heavily glycosylated gp120 compared with the other glycoproteins.[16,46]

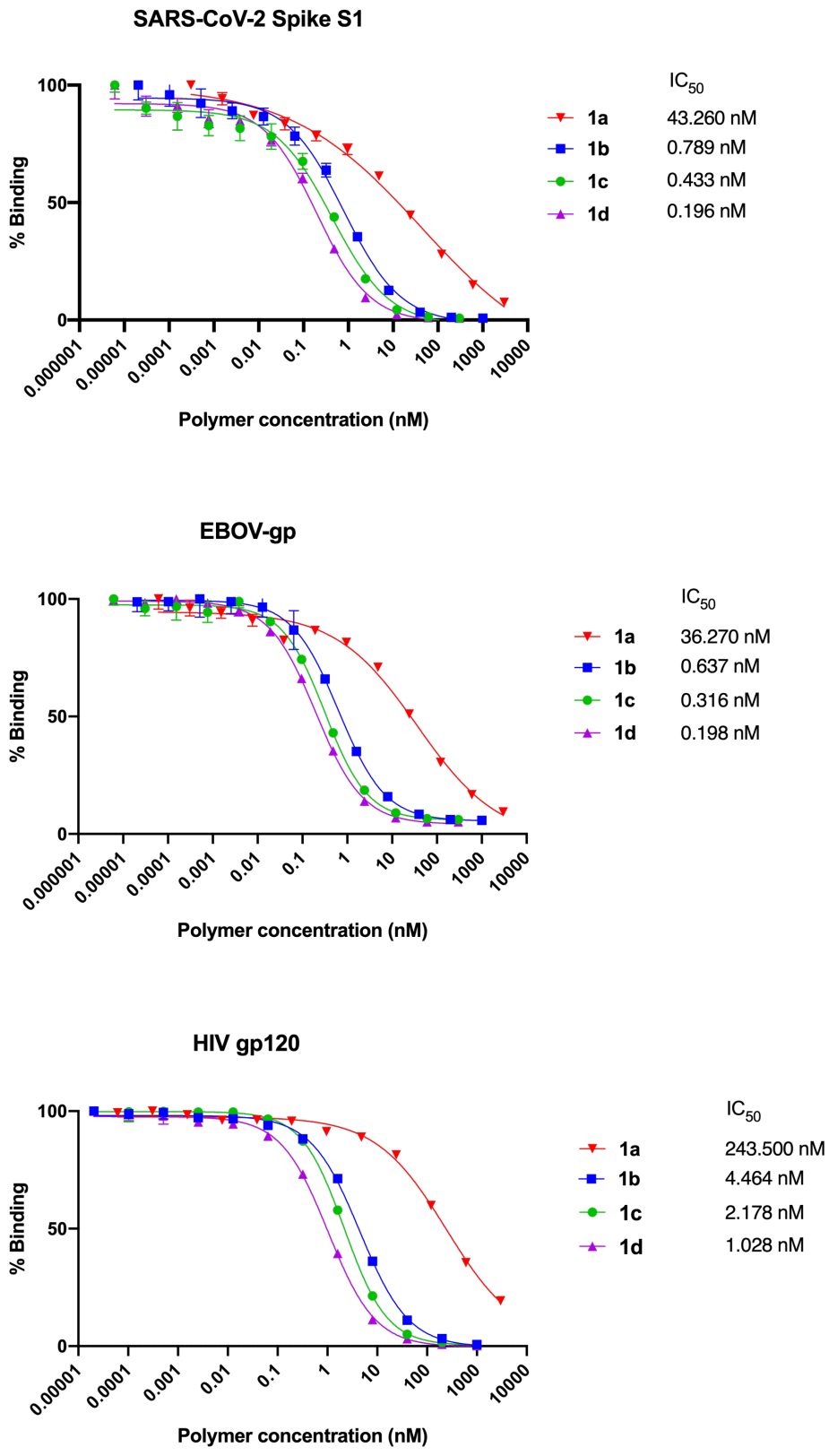

Figure 2. Inhibition of viral glycoprotein attachment to DC-SIGN⁺ B-THP-1 cells. Cells were incubated with Man-PLL **1a-d** in the presence of Cy5 labeled SARS-CoV-2 spike glycoprotein S1 subunit (10 nM), ebola

glycoprotein (50 nM), or HIV gp120 (10 nM). Mean fluorescence intensity determined by flow cytometry was normalized before global fitting to a four parameter Hill model. Error bars represent the standard deviation from three independent experiments.

Intriguingly, the observed trend in affinity in the cellular assay correlates well with the solution properties of the Man-PLL glycopolymers determined by DLS and AUC (Table 2, Figure 1). The differences in size and shape are reflected in a significantly higher binding affinity (approximately a factor of 50) of elongated polymers **1b-d** in cellular assays compared with the globular **1a**. By comparison, between **1b-d**, the variations in the degree of polymerization (**1b** → **1c**) and carbohydrate loading (**1c** → **1d**) influences affinity only by a factor of two. The observation that the elongated glycopolymers **1b-d** show much higher affinity compared to the globular **1a** is probably related to the fact that DC-SIGN has evolved to capture large pathogens, such as viruses (ca. 20–500 nm) or bacteria (1–2 μm), and not soluble glycoproteins. A similar influence of particle size of antigen formulations on DC-SIGN affinity and antigen uptake has been reported by the van Kooyk group.[47]

Prolonged incubation of DC-SIGN$^+$ B-THP-1 cells with the most potent inhibitor **1d** effectively blocked the DC-SIGN receptors, making them unavailable for binding to SARS-CoV-2 spike S1 for up to 6 h (Figure 3A). An effect could still be observed after only a 30 min exposure of the cells (Figure 3B). Whereas inhibition was incomplete compared to a prolonged exposure to Man-PLL$_{400}$ (**1d**), the binding of SARS-CoV-2 spike S1 was still significantly decreased for up to 6 h post incubation.

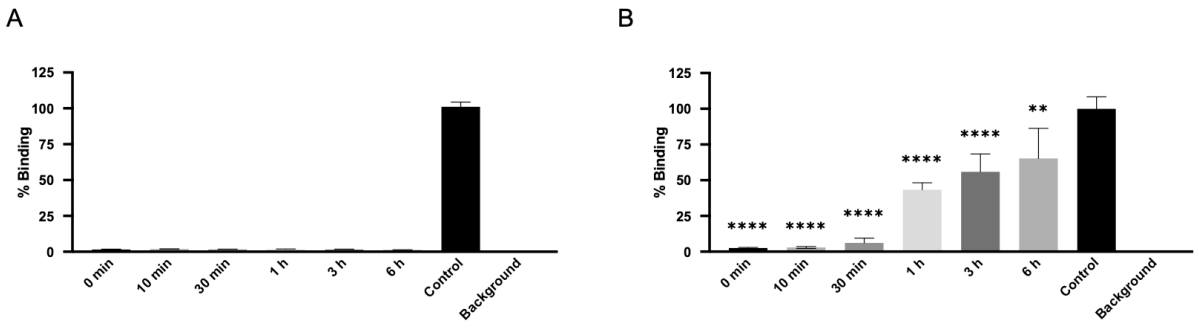

Figure 3. Inhibition of the DC-SIGN receptor on B-THP-1 cells by **1d**. A) Incubation of the cells with 100 nM **1d** lead to a sustained blocking of the DC-SIGN receptor for at least 6 hours, thereby successfully preventing the binding of Cy5 labeled SARS-CoV-2 spike glycoprotein S1 subunit (10 nM). B) Pre-incubation of the cells with 100 nM **1d** for 30 min showed a time dependent recovery of the receptor with a significantly decreased binding availability for at least 6h. Results are shown as mean with standard deviation from three independent experiments (one-way ANOVA, *P ≤ 0.05, **P ≤ 0.01, ***P ≤ 0.001, ****P ≤ 0.0001).

Uptake of Man-PLL 1a-d into target cells

To study endocytosis into acidic cell compartments by flow cytometry and fluorescence microscopy, Man-PLL_{400} was labeled with the pH-sensitive fluorescent dye rhodamine 6G (Man loading: 47% by NMR, for synthesis of **10**, see Supporting Information). As negative control, the fluorescently labeled PLL_{400} **11** containing no mannose modification was used (for synthesis of **11**, see Supporting Information). Both polymers were incubated with DC-SIGN$^+$ B-THP-1 cells and control B-THP-1 cells. Fluorescently labeled Man-PLL_{400} **10** was internalized highly specifically by DC-SIGN expressing B-THP-1 cells (Figure 4A) and the fluorescent signal increased over 6 h and diminished after 24 h hours, highlighting a complete degradation of the compound as previously described by Hoppe and Lee.[44] In contrast, no uptake was observed in control B-THP-1 cells and only minor uptake of non-mannosylated control PLL_{400} **11** into both cell types was observed (Figure 4)

These observations further elucidate the mode of action of the Man-PLL. Multivalent binding to DC-SIGN on the cell surface causes effective inhibition of the binding of viral glycoproteins. Additionally, the compound is readily endocytosed via DC-SIGN. As a result, the availability of DC-SIGN on the cell surface is substantially reduced, and the glycopolymers are efficiently metabolized (Figure 4B).

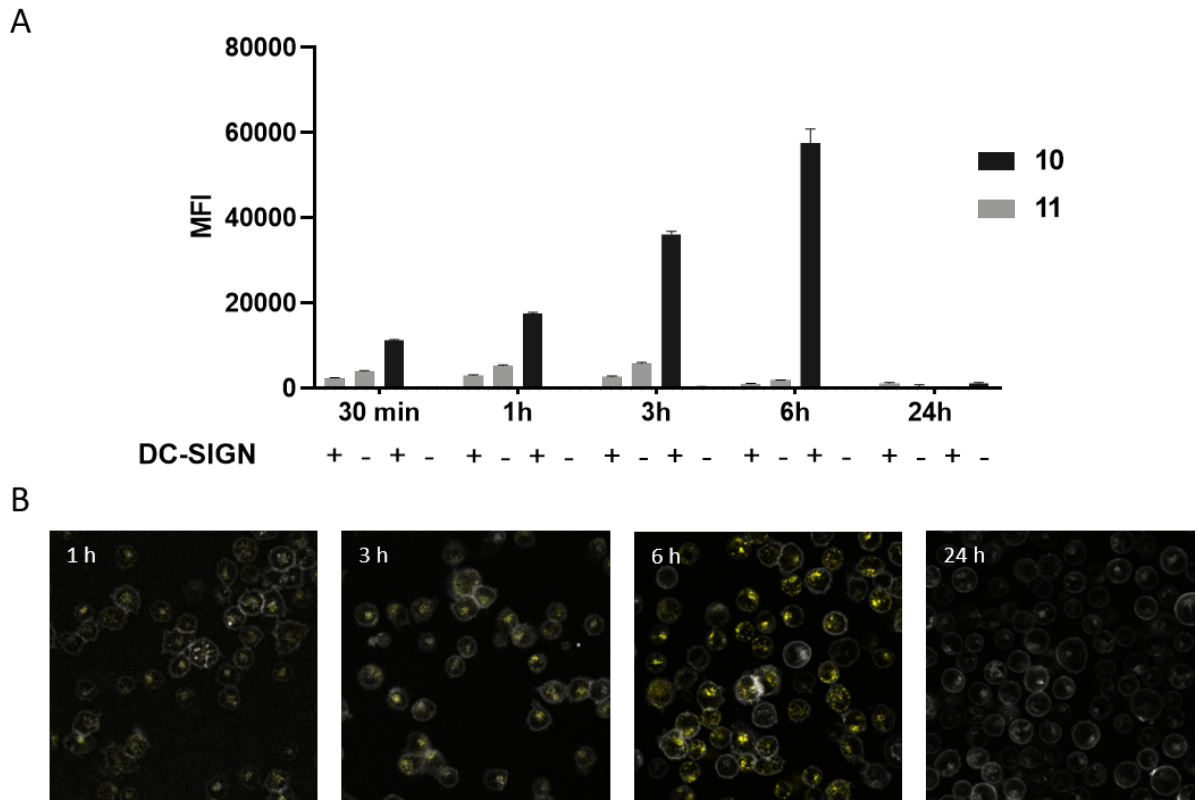

Figure 4. DC-SIGN mediated uptake and degradation of fluorescently labeled Man-PLL$_{400}$ **10** into B-THP-1 cells. DC-SIGN$^+$ B-THP-1 cells and control B-THP-1 cells were incubated with 100 nM rhodamine 6G labeled Man-PLL$_{400}$ **10** or 100 nM rhodamine 6G labeled PLL$_{400}$ **11**. A) The internalization was quantified by measuring the pH-dependent mean fluorescence intensity with flow cytometry, showing the highly specific and time-dependent uptake of **10** by DC-SIGN$^+$ B-THP-1 cells (+) in comparison to control B-THP-1 cells (-) and control **11**. Furthermore, after increasing fluorescence intensity over time, the signal disappeared after 24 h, highlighting the targeted uptake and degradation. B) Representative images recorded with confocal microscopy reveal the time dependent uptake of **10** in acidic cell compartments of DC-SIGN$^+$ B-THP-1 cells and the effective degradation after 24 h. Error bars represent the standard deviation from three independent experiments.

Analysis of binding thermodynamics

Whereas the above discussed competitive cell assay yields data about the potency of Man-PLL **1a-d**, it does not provide detailed information about the specifics of the interaction on a molecular level. To gain more insight into molecular details of the Man-PLL/DC-SIGN

interaction, the affinity, stoichiometry (*n*), and thermodynamics of binding were determined by isothermal titration calorimetry (ITC) with the tetrameric recombinant extracellular domain of DC-SIGN (ECD, 375 amino acids). It is important to note that this biophysical assay operates under a fundamentally different principle compared to the cellular assay. The ITC experiment records the interaction of soluble tetrameric DC-SIGN molecules with the polymeric ligands, whereas in the cellular assay the interaction of two mutually compatible multivalent surfaces is studied. In contrast to the affinity data determined in the cellular assay, a linear increase of the binding affinity K_D (Figure 5) from **1a** to **1d** was observed in the ITC experiment. Compared to the monovalent ligand MeMan (K_D = 3.2 mM), the multivalent presentation enhances affinity by a factor of 2.6×10^3 for **1a** and up to a factor of 13.5×10^3 for **1d**. This difference in the multivalent affinity enhancement between the cellular assay and the interaction of the glycopolymers with soluble lectin receptors (see Figure 2 and 5) can be attributed to the multivalent presentation of receptor molecules on the cell surface, which effectively potentiates the affinity enhancement from statistical rebinding by providing a much higher effective local concentration of receptors. While an equivalent affinity trend is observable in ITC experiments and the cellular assay, the difference between **1a** and **1b**-**1d** is much less pronounced in the ITC assay with soluble protein (factor of 3-5) compared with the cellular assay (factor of 50-200), indicating that Man-PLL shape and hydrodynamic diameter are better predictors for activity in a cellular system than binding affinity from ITC. In summary, this observation indicates that, on the cellular level, the interaction with DC-SIGN is controlled by effects that are not fully reproduced in a biophysical assay employing soluble recombinant protein.

The affinity trend in ITC measurements roughly follows the increase of the functional valency *N*, which is defined as the inverse of the experimentally determined fitting parameter *n* ($N = 1/n$) and corresponds to the number of interacting mannose epitopes on the glycopolymer. *N* can be related to the total number N_{max} of mannose epitopes on the respective polymer. With

an N/N_{max} of 109% and 93%, the mannose epitopes of the shorter polymers **1a** and **1b** appear to be fully saturated, whereas only a fraction of available mannose residues in the longer polymers **1c** and **1d** bind to the receptor (with N/N_{max} 58% and 48%, respectively). Taking into account the broad distribution of high MW species in AUC experiments (Figure 1A), it is likely that self-aggregation reduces the accessibility of sugar residues on the Man-PLL$_{400}$ **1c** and **1d**. The reduction of the active mannose concentration in the samples is reflected in the ITC fitting parameter *n*, which leads to a reduced value of N/N_{max}. A similar reduction of efficiency related to higher carbohydrate loading, not polymer length as in this case, has been observed for other glycopolymers.[48–51] Interestingly, aggregation does not reduce the availability of mannose epitopes on the polymer surface for **1b**. The intermediate length polymer is, thus, most efficient in terms of affinity gain per carbohydrate epitope on the polymer.

	1a	**1b**	**1c**	**1d**
K_D [nM]	1227 (1034 – 1474)	432 (406 – 460)	352 (284 – 438)	235 (205 – 269)
N	48 (42 – 57)	102 (97 – 109)	90 (85 – 97)	118 (114 – 123)
N_{max}	44	110	156	248
N/N_{max}[%]	109	93	58	48

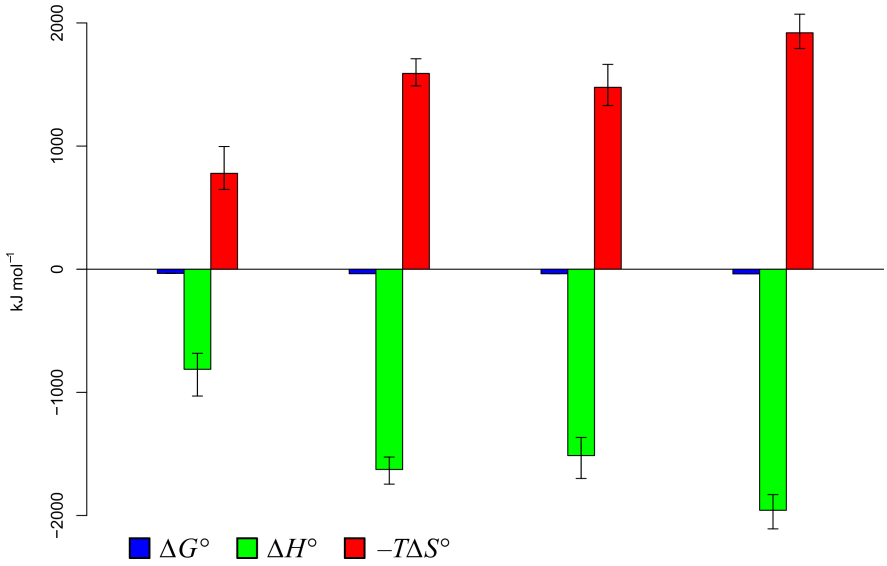

Figure 5. Thermodynamic fingerprints of the interaction of glycopolymers **1a**-**d** with DC-SIGN ECD. The functional valency *N* is the inverse of the fitting parameter *n* determined in ITC experiments; N_{max} equals the total

number of mannose epitopes on polymer. Thermodynamic data in numeric form can be found in the Supporting Information.

Similar to the binding affinity, the observed entropy-enthalpy compensation in the ITC experiments scales with the fitting parameter *n* and thus with the functional valency *N* (*N* = 1/*n*). Figure 6 depicts a plot of the thermodynamic profiles normalized by functional valency *N* of the interaction. These fingerprints reflect the contribution of each interacting mannose residue of the multivalent glycoconjugates. For comparison, the thermodynamic profile of the monovalent ligand MeMan was included in the plot. Compared with the monovalent interaction, the multivalency effect enhances the normalized binding affinities of **1a-d** by a factor of 54 to 113 (K_D MeMan/K_D Man-PLL). The thermodynamic profile of MeMan reveals an enthalpy-driven interaction ($\Delta H^{\circ}_{norm} = -17.4\ kJ\ mol^{-1}$) that is partly compensated by an entropic penalty of $-T\Delta S^{\circ}_{norm} = 3.1\ kJ\ mol^{-1}$. Intriguingly, the normalized thermodynamic profiles for Man-PLL **1a-d** are identical to each other within the error of the experiment. All glycopolymers display an enthalpically favorable interaction ($\Delta H^{\circ}_{norm} \approx -17\ kJ\ mol^{-1}$) with a similarly favorable entropic contribution ($-T\Delta S^{\circ}_{norm} \approx -9\ kJ\ mol^{-1}$). Thus, the observed affinity gain relative to MeMan is entirely related to a reduction of the entropic penalty for each carbohydrate epitope by 12 kJ mol^{-1} on average, whereas binding enthalpy essentially remains unchanged. Interestingly, this value is fairly close to the rigid body entropic barrier for fragment linking of 15-20 kJ mol^{-1} postulated by Murray and Verdonk.[52] However, multivalent effects related to ligand entropy are likely superimposed by additional contributions from modification of polymer backbone flexibility upon binding.

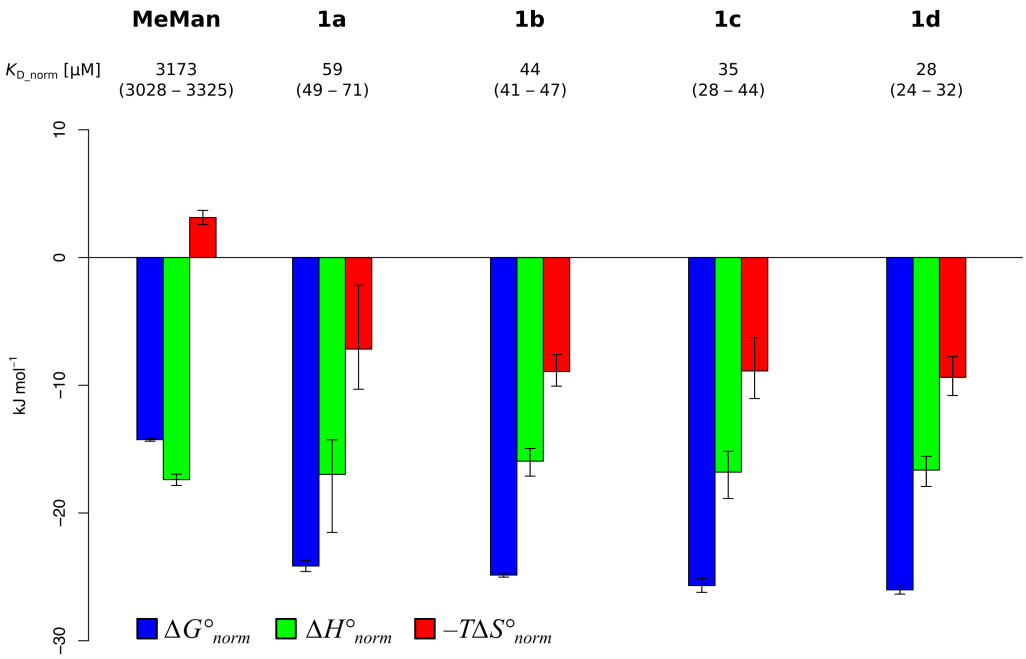

Figure 6. Normalized affinity and thermodynamic profile of MeMan and Man-PLL **1a-d** ($\Delta G^{\circ}_{norm} = \Delta G^{\circ} \times n$; $\Delta H^{\circ}_{norm} = \Delta H^{\circ} \times n$; $-T\Delta S^{\circ}_{norm} = -T\Delta S^{\circ} \times n$; $K_{D\_norm} = e^{\frac{\Delta G^{\circ}_{norm}}{RT}}$). Thermodynamic data in numeric form can be found in the Supporting Information.

The thermodynamics of multivalent ligands binding to lectins are often associated with an enhancement of binding entropy.[30,31,53] The initial association of the ligand suffers from an entropic penalty due to its loss of translational and rotational degrees of freedom. In contrast to monovalent interactions, no additional entropy costs arise from the interaction of further epitopes of the multivalent construct. This effect can be equivalently described as a change of the ligand concentration in the unbound state from the standard concentration for the monovalent interaction to a higher effective concentration in multivalent systems.[54,55] Thus, multivalent enhancement effects from statistical rebinding are essentially an entropic phenomenon, whereas the binding enthalpy of each individual interaction on a multivalent system resembles the monovalent interaction. This strongly suggests that the introduction of glycomimetic ligands with an improved enthalpic signature holds the potential to significantly

increase binding affinity of glycopolymers. Hypothetically, even small gains in monovalent binding enthalpy will be significantly enhanced by the multivalency effect.

Conclusions

In this study, we demonstrate that Man-PLL glycopolymers **1a**-**d** potently inhibit the attachment of viral envelope glycoproteins to DC-SIGN$^+$ cells. The presentation of mannose epitopes on the PLL scaffold resulted in a multivalent affinity enhancement of up to 10^7. Intriguingly, the affinity of the polymers is strongly correlated with the size and shape of the molecular particles in solution. Large, elongated molecules (**1b**-**d**) were found to be more potent inhibitors of viral glycoprotein binding compared with the smaller, globular polymer **1a**, probably because in elongated molecules the availability of epitopes for binding to a cell surface is spatially favored. Importantly, treatment of DC-SIGN$^+$ cells with Man-PLL **1d** lead to a prolonged inhibition of SARS-CoV-2 spike S1 binding, highlighting the therapeutic potential of this approach.

A thermodynamic analysis of the Man-PLL/DC-SIGN interaction revealed that the multivalent affinity enhancement is mainly driven by an entropic advantage of 12 kJ mol^{-1}, which is related to the reduction of translational and rigid body rotational entropy costs. At the same time, the enthalpic contribution of each interacting mannose on the polymer corresponds roughly to the value obtained for the monovalent interaction. This finding has important implications for the future design of glycopolymers and other multivalent glycomaterials. The presentation of glycomimetics with increased monovalent binding enthalpy on a multivalent support holds the potential to further improve potency and selectivity for lectin binding.

Efficient clearance of nanometer-sized polymeric therapeutics is a prerequisite for a prolonged pulmonary application without compound accumulation and associated toxicity. We demonstrated that fully bio-compatible Man-PLL polymers are efficiently internalized and

degraded by their target cells and, thus, are unlikely to accumulate in lung tissue after inhalation.

With respect to the ongoing SARS-CoV-2 pandemic, DC-SIGN targeted Man-PLL polymers represent a novel treatment option for severe COVID-19, which is characterized by an exuberant immune response with the release of pro-inflammatory cytokines. Inhibition of the DC-SIGN-mediated infection of myeloid cells by pulmonary application of Man-PLL may be able to prevent progression of mild infections to severe forms of the disease.

Experimental Part

Synthesis

General methods: NMR spectra were recorded on a Bruker Avance III 500 MHz spectrometer. Assignment of ^{1}H and ^{13}C NMR spectra was achieved using 2D methods (COSY, HSQC, HMBC). Chemical shifts are expressed in ppm using residual $CHCl_3$, CHD_2OD or HDO as references. Electron spray ionization mass spectra (ESI-MS) were obtained on a Waters micromass ZQ Mass Spectrometer. Reactions were monitored by TLC using glass plates coated with silica gel 60 F_{254} (Merck, Darmstadt, Germany) and visualized by using UV light and/or by charring with a molybdate solution (a 0.02 M solution of ammonium cerium sulfate dihydrate and ammonium molybdate tetrahydrate in aqueous 10% H_2SO_4). MPLC separations were carried out on a CombiFlash Companion or R_f from Teledyne Isco (Lincoln, NE, USA) equipped with RediSep flash columns. For purification of glycopolymers, Vivaspin ultrafiltration devices with a molecular weight cutoff of 6 kDa or 50 kDa (Sartorius, Göttingen, Germany) were used. Commercially available reagents and dry solvents were purchased from Sigma-Aldrich, Alfa Aesar and Acros Organics. Poly-L-lysine HBr polymers were acquired from PtS (Valencia, Spain).

For the synthesis of the mannose building block **4**, fluorescently labeled Man-PLL_{400} **10**, fluorescently labeled PLL_{400} **11** and the preparation of the chloroacetyleted poly-L-lysinse **3a-c** see Supporting Informations.

General method for the synthesis of Man-PLL glycopolymers

Chloroacetylated poly-L-lysine **3a-c** (1 eq) was dissolved in DMF (0.3 mL) under an Argon atmosphere. To this 1,8-diazabicyclo[5.4.0]undec-7-en (DBU, 400 eq) and a solution of mannose derivative **4** in 30 μL H_2O was added and the resulting mixture was shaken for 60 min at rt. Thioglycerol (1200 eq) and triethylamine (1200 eq) were added and shaking at rt was continued overnight. The mixture was poured into a vigorously stirred 1:1 mixture of EtOH and EtOAc (4 mL), which resulted in the precipitation of the polymer. After centrifugation (1000 rpm, 2 min, 4 °C), the supernatant was discarded and the precipitate was washed with 3 mL EtOH. The crude product was dissolved in 3 mL H_2O and purified by ultrafiltration using a Vivaspin centrifugal concentrator (Sartorius, Germany; 6 mL, MWCO 6 kDa or 50 kDa). Lyophilization gave the pure product as a colorless solid. Mannose loading was determined by NMR by comparing the integrals of thioglycerol CH_2-SR and mannoside CH_2-SR/CH_2-CONH.

*Synthesis of Man-PLL **1a***

According to general method using chloroacetylated poly-L-lysine **3a** (4.7 mg, 230 nmol, 1 eq), DBU (14.0 mg, 92 µmol, 400 eq), mannose derivative **4** (3.5 mg, 10 µmol, 44 eq), thioglycerol (7.5 mg, 69 µmol, 300 eq), and triethylamine (7.0 mg, 69 µmol, 300 eq). The product **1a** was obtained as a colorless solid (3.9 mg, 103 nmol, 45%). Mannose loading by NMR (see Supporting Information, Figure S1): 44%.

*Synthesis of Man-PLL **1b***

According to general method using chloroacetylated poly-L-lysine **3b** (3.6 mg, 70 nmol, 1 eq), DBU (2.7 mg, 18 µmol, 257 eq), mannose derivative **4** (2.7 mg, 9 µmol, 127 eq), thioglycerol (5.7 mg, 53 µmol, 757 eq), and triethylamine (5.4 mg, 53 µmol, 757 eq). The product **1b** was obtained as a colorless solid (4.3 mg, 45 nmol, 64%). Mannose loading by NMR (see Supporting Information, Figure S2): 46%.

*Synthesis of Man-PLL **1c***

According to general method using chloroacetylated poly-L-lysine **3c** (5.7 mg, 70 nmol, 1 eq), DBU (4.3 mg, 28 µmol, 400 eq), mannose derivative **4** (3.3 mg, 10 µmol, 143 eq), thioglycerol (9.1 mg, 84 µmol, 1200 eq), and triethylamine (8.5 mg, 84 µmol, 1200 eq). The product **1c** was obtained as a colorless solid (7.0 mg, 48 nmol, 68%). Mannose loading by NMR (see Supporting Information, Figure S3): 39%.

*Synthesis of Man-PLL **1d***

According to general method using chloroacetylated poly-L-lysine **3c** (4.2 mg, 50 nmol, 1 eq), DBU (3.0 mg, 20 µmol, 400 eq), mannose derivative **4** (3.1 mg, 9 µmol, 180 eq), thioglycerol (6.5 mg, 60 µmol, 1200 eq), and triethylamine (6.1 mg, 60 µmol, 1200 eq). The product **1d** was obtained as a colorless solid (4.3 mg, 26 nmol, 51%). Mannose loading by NMR (see Supporting Information, Figure S4): 62%.

Protein expression and purification

E. coli BL21(DE3) cells were transfected with Novagen pET15b plasmids encoding for a recombinant DC-SIGN ECD linked to a thrombin cleavage site and an N-terminal His-Tag. Cells were initially cultivated overnight in 20 mL Luria Bertani medium substituted with 0.1 mg/mL ampicillin at 37 °C and then transferred into 1 L Terrific Broth medium substituted with 0.1 mg/mL ampicillin. Cells were incubated for 8 h at 37 °C and DC-SIGN expression was

induced by addition of 0.5 mM IPTG. After 16 h, cells were harvested by centrifugation (4,000 rpm, 20 min, 4 °C), resuspended in lysis buffer (50 mM Tris-HCl, 10 mM $MgCl_2$, 0.1% Triton X100), and lysed by sonication or addition of lysozyme and DNAse I. The cell lysate was centrifuged (11000 rpm, 20 min, 4 °C), the supernatant discarded, and the precipitated material was washed three times with washing buffer (50 mM Tris–HCl, pH 8.0, 4 M urea, 500 mM NaCl, 1 mM EDTA). The purified inclusion bodies were dissolved in 20 mL of denaturation buffer (6 M guanidine hydrochloride, 100 mM Tris–HCl, pH 8.0, 1 mM DTT) for 1 h at 37 °C. After ultracentrifugation (22000 rpm, 30 min, 4 °C), the denatured protein was refolded by slow dilution into 100 mL refolding buffer (100 mM Tris–HCl, pH 8.0, 1 M l-arginine, 150 mM NaCl, 120 mM sucrose). The mixture was stirred for 2 d at 4 °C and dialyzed against binding buffer (20 mM Tris-HCl, 500 mM NaCl, 25 mM $CaCl_2$, pH 7.8). Precipitated protein was removed by ultracentrifugation (22000 rpm, 30 min, 4 °C) and the refolded soluble protein was purified by affinity chromatography on a mannose-sepharose column (elution buffer: 20 mM TRIS, 500 mM NaCl, 2 mM EDTA, pH 7.8).

Isothermal titration calorimetry

A MicroCal ITC200 instrument (MicroCal, Northampton, USA) was used for all ITC experiments. All measurements were performed at 25 °C using a reference power of 6 µcal s^{-1}, a stirring speed of 750 rpm, feedback mode high, and a filter period of 2 s. Prior to the experiments, all protein samples were extensively dialyzed against ITC buffer (20 mM HEPES, 150 mM NaCl, 1 mM $CaCl_2$, pH 7.4) and all non-protein samples were prepared using the dialysate buffer to minimize dilution effects. Protein concentration was determined photometrically with absorbance at 280 nm employing a calculated extinction coefficient of 70400 mol^{-1} cm^{-1}. In a typical experiment, a glycoconjugate sample (20 – 50 µM) was titrated into 50 µM DC-SIGN ECD. The concentration of the glycoconjugate sample was chosen to ensure sufficient protein saturation (> 80%) at the end of the experiment. A control titration

was performed for experiments with large observed dilution enthalpies and experimental data was corrected by subtraction of the blank values. In general, experimental data could be used directly without correction, in which case enthalpy of dilution was included as a separate fitting parameter. Baseline correction and integration was performed with NITPIC.[56,57] Sedphat was used for nonlinear regression analysis of experimental data, determination of confidence intervals, and calculation of two-dimensional error surface projections.[57,58]

Dynamic light scattering

The size characteristics of Man-PLL **1a-d** were analyzed by DLS with a Malvern Zetasizer Nano instrument (Malvern Panalytical, Malvern, UK). Samples containing 10 µM **1a** (0.38 mg mL^{-1}) or 2 µM **1b-d** (0.02-0.34 mg mL^{-1}) were allowed to equilibrate at 20 °C for two minutes prior to the experiments. Experiments were performed in triplicate and experimental data were analyzed with the manufacturer supplied software to obtain hydrodynamic radii (Z-average), polydispersity indices, and size distribution data.

Analytical ultracentrifugation

Sedimentation velocity experiments were performed for 410 µl samples at concentrations of 0.8 mg ml^{-1} (22 µM) for Man-PLL **1a**, 0.2 mg ml^{-1} (2 µM) for Man-PLL **1b**, 1.3 mg ml^{-1} (9 µM) for Man-PLL **1c**, and 0.2 mg ml^{-1} (1 µM) for Man-PLL **1d** at 20 °C in 20 mM HEPES, 150 mM NaCl, 1 mM $CaCl_2$, pH 7.4. Centrifugation was performed at 42,000 rpm (128,000 x g) using a Beckman XL-I Analytical Ultracentrifuge with an An-60 Ti rotor, and sedimentation was monitored using the interference optics with 12 mm double-sector charcoal-epon centerpieces. The data were analysed by fitting diffusion-deconvoluted differential sedimentation coefficient distributions (c(s) distributions) using the program SEDFIT,[59] best-fit values of the frictional ratio (f/f_0), meniscus and bottom positions, and time- and radially-invariant noise profiles were determined for each data set. Values of buffer density and viscosity

were obtained from Sednterp.[60] Values of partial specific volume were calculated for individual components of Man-PLLs **1a-d**, namely lysine conjugated to mannose (0.797 ml g^{-1}) and for lysine conjugated to thioglycerol (0.772 ml g^{-1}) using the method of Durchschlag and Zipper.[61] Partial specific volumes were then calculated for different polymers according to estimated mass fraction of mannose or thioglycerol conjugated lysine in the polymer (0.787 ml g^{-1} for Man-PLL **1a**, 0.787 ml g^{-1} for Man-PLL **1b**, 0.786 ml g^{-1} for Man-PLL **1c**, and 0.790 ml g^{-1} for Man-PLL **1d**. Signal-weighted average S values were calculated from c(s) distributions using the program GUSSI.[62] Values of D_h were calculated from diffusion coefficients, which in turn were calculated from signal-weighted average S values and f/f_0 according to a standard scaling law.[63]

Mammalian cell culture, flow cytometry, and fluorescence microscopy

The following reagents were obtained through the NIH AIDS Reagent Program, Division of AIDS, NIAID, NIH: B-THP-1 DC-SIGN+ cells from Drs. Li Wu and Vineet N. KewalRamani (cat# 9941),[64] HIV-1 JR-CSF Fc-gp120 Recombinant Protein (Cat#11556) from Aymeric de Parseval and Dr. John H. Elder.[65] Recombinant ebola glycoprotein was obtained from R&D Systems (cat# 9016-EB-100), recombinant SARS-CoV-2 spike glycoprotein S1 subunit was purchased from Creative Biomart (cat# Spike-191V).

Cells were maintained in RPMI 1640 medium substituted with 10 % FCS at 37 °C. For IC50 measurements, 50000 cells were seeded in 50 µL complete medium in a well of a 96-well plate. A serial dilution of the investigated ligand was prepared and mixed with an equal volume of Cy5-labeled glycoprotein. This mixture was added to the cell suspension to a final volume of 100 µL and a final glycoprotein concentration of 10 nM (gp120), 10 nM (SARS-CoV-2 spike S1), or 50 nM (EBOV-gp). After incubation for 30 min (37°C, 5 % CO_2), the cells were centrifuged (5 min, 100g) and washed with warm PBS. Data were collected on a Cytoflex flow cytometer (Beckman Coulter, Indianapolis, USA) and analyzed with FlowJo (FlowJo LLC).

Mean fluorescence intensities were plotted and a nonlinear regression analysis employing a four parameter Hill model was performed with Prism 8 (Graphpad, San Diego, USA). For receptor blocking analysis, 50000 B-THP-1 DC-SIGN$^+$ cells were seeded and incubated with 100 nM **1d** for 0 min to 6h, before washing and incubation with Cy5-labeled recombinant SARS-CoV-2 spike glycoprotein S1 subunit according to the protocol of the IC_{50} measurements. Additionally, B-THP-1 DC-SIGN$^+$ cells were incubated with 100 nM **1d** for 30 min, washed, and incubated with Cy5-labeled recombinant SARS-CoV-2 spike glycoprotein S1 subunit after 0 min, 10 min, 30 min, 1h, 3h, and 6h. Internalization experiments were performed with B-THP-1 DC-SIGN$^+$ cells and control B-THP-1 cells. 50000 cells were incubated with 100 nM **10** and 100 nM **11** for 30 min, 1h, 3h, 6h, and 24h, washed with PBS, and analyzed by flow cytometry. For microscopic analysis cells were additionally incubated with 5 µg/ml CellMask Deep Red Plasma membrane stain (C10046, Invitrogen, Thermo Fisher Scientific, Switzerland) for 10 min. Images were recorded with the Leica SP8 confocal point scanning microscope using a HC PL Apo CS 40x (NA 1.1) objective (Leica Microsystems, Germany). Comparisons between the conditions were performed using one-way ANOVA with Dunnett's multiple comparison posttest with a 0.05 confidence level accepted for statistical significance (*$P \leq 0.05$, **$P \leq 0.01$, ***$P \leq 0.001$, ****$P \leq 0.0001$).

Supporting Information

Electronic Supporting Information is available free of charge on the ACS website. Synthesis of polymer precursors, NMR characterization of **1a**–**d**, additional information on ITC titrations, calculation of equilibrium concentrations, thermodynamic data, thermograms, sedimentation velocity data from AUC.

References

(1) Monteiro, J.; Lepenies, B. Myeloid C-Type Lectin Receptors in Viral Recognition and Antiviral Immunity. *Viruses* **2017**, *9* (3), 59.

(2) Bermejo-Jambrina, M.; Eder, J.; Helgers, L. C.; Hertoghs, N.; Nijmeijer, B. M.; Stunnenberg, M.; Geijtenbeek, T. B. H. C-Type Lectin Receptors in Antiviral Immunity and Viral Escape. *Front. Immunol.* **2018**, *9* (MAR), 590.

(3) Garcia-Vallejo, J. J.; van Kooyk, Y. DC-SIGN: The Strange Case of Dr. Jekyll and Mr. Hyde. *Immunity* **2015**, *42* (6), 983–985.

(4) van Kooyk, Y.; Geijtenbeek, T. B. H. DC-SIGN: Escape Mechanism for Pathogens. *Nat. Rev. Immunol.* **2003**, *3* (9), 697–709.

(5) Martín-Moreno, A.; Muñoz-Fernández, M. A. Dendritic Cells, the Double Agent in the War Against HIV-1. *Front. Immunol.* **2019**, *10* (OCT), 2485.

(6) Marzi, A.; Möller, P.; Hanna, S. L.; Harrer, T.; Eisemann, J.; Steinkasserer, A.; Becker, S.; Baribaud, F.; Pöhlmann, S. Analysis of the Interaction of Ebola Virus Glycoprotein with DC-SIGN (Dendritic Cell–Specific Intercellular Adhesion Molecule 3–Grabbing Nonintegrin) and Its Homologue DC-SIGNR. *J. Infect. Dis.* **2007**, *196* (s2), S237–S246.

(7) Simmons, G.; Reeves, J. D.; Grogan, C. C.; Vandenberghe, L. H.; Baribaud, F.; Whitbeck, J. C.; Burke, E.; Buchmeier, M. J.; Soilleux, E. J.; Riley, J. L.; et al. DC-SIGN and DC-SIGNR Bind Ebola Glycoproteins and Enhance Infection of Macrophages and Endothelial Cells. *Virology* **2003**, *305* (1), 115–123.

(8) Hillaire, M. L. B.; Nieuwkoop, N. J.; Boon, A. C. M.; de Mutsert, G.; Vogelzang-van Trierum, S. E.; Fouchier, R. A. M.; Osterhaus, A. D. M. E.; Rimmelzwaan, G. F. Binding of DC-SIGN to the Hemagglutinin of Influenza A Viruses Supports Virus Replication in DC-SIGN Expressing Cells. *PLoS One* **2013**, *8* (2), e56164.

(9) Pöhlmann, S.; Zhang, J.; Baribaud, F.; Chen, Z.; Leslie, G. J.; Lin, G.; Granelli-Piperno, A.; Doms, R. W.; Rice, C. M.; McKeating, J. A. Hepatitis C Virus Glycoproteins Interact with DC-SIGN and DC-SIGNR. *J. Virol.* **2003**, *77* (7), 4070–4080.

(10) Marzi, A.; Gramberg, T.; Simmons, G.; Moller, P.; Rennekamp, A. J.; Krumbiegel, M.; Geier, M.; Eisemann, J.; Turza, N.; Saunier, B.; et al. DC-SIGN and DC-SIGNR Interact with the Glycoprotein of Marburg Virus and the S Protein of Severe Acute Respiratory Syndrome Coronavirus. *J. Virol.* **2004**, *78* (21), 12090–12095.

(11) Routhu, N. K.; Lehoux, S. D.; Rouse, E. A.; Bidokhti, M. R. M.; Giron, L. B.; Anzurez, A.; Reid, S. P.; Abdel-Mohsen, M.; Cummings, R. D.; Byrareddy, S. N. Glycosylation of Zika Virus Is Important in Host–Virus Interaction and Pathogenic Potential. *Int. J. Mol. Sci.* **2019**, *20* (20), 5206.

(12) Tassaneetrithep, B.; Burgess, T. H.; Granelli-Piperno, A.; Trumpfheller, C.; Finke, J.; Sun, W.; Eller, M. A.; Pattanapanyasat, K.; Sarasombath, S.; Birx, D. L.; et al. DC-SIGN

(CD209) Mediates Dengue Virus Infection of Human Dendritic Cells. *J. Exp. Med.* **2003**, *197* (7), 823–829.

(13) Yang, Z.-Y.; Huang, Y.; Ganesh, L.; Leung, K.; Kong, W.-P.; Schwartz, O.; Subbarao, K.; Nabel, G. J. PH-Dependent Entry of Severe Acute Respiratory Syndrome Coronavirus Is Mediated by the Spike Glycoprotein and Enhanced by Dendritic Cell Transfer through DC-SIGN. *J. Virol.* **2004**, *78* (11), 5642–5650.

(14) Colmenares, M.; Puig-Kröger, A.; Pello, O. M.; Corbí, A. L.; Rivas, L. Dendritic Cell (DC)-Specific Intercellular Adhesion Molecule 3 (ICAM-3)-Grabbing Nonintegrin (DC-SIGN, CD209), a C-Type Surface Lectin in Human DCs, Is a Receptor for Leishmania Amastigotes. *J. Biol. Chem.* **2002**, *277* (39), 36766–36769.

(15) Brufsky, A.; Lotze, M. T. DC/L-SIGNs of Hope in the COVID-19 Pandemic. *J. Med. Virol.* **2020**, jmv.25980.

(16) Watanabe, Y.; Allen, J. D.; Wrapp, D.; McLellan, J. S.; Crispin, M. Site-Specific Glycan Analysis of the SARS-CoV-2 Spike. *Science (80-.).* **2020**, eabb9983.

(17) Gao, C.; Zeng, J.; Jia, N.; Stavenhagen, K.; Matsumoto, Y.; Zhang, H.; Li, J.; Hume, A. J.; Muehlberger, E.; van Die, I.; et al. SARS-CoV-2 Spike Protein Interacts with Multiple Innate Immune Receptors. *bioRxiv* **2020**, 2020.07.29.227462.

(18) Amraie, R.; Napoleon, M. A.; Yin, W.; Berrigan, J.; Suder, E.; Zhao, G.; Olejnik, J.; Gummuluru, S.; Muhlberger, E.; Chitalia, V.; et al. CD209L/L-SIGN and CD209/DC-SIGN Act as Receptors for SARS-CoV-2 and Are Differentially Expressed in Lung and Kidney Epithelial and Endothelial Cells. *Biorxiv* **2020**, 2020.06.22.165803.

(19) Amraei, R.; Rahimi, N. COVID-19, Renin-Angiotensin System and Endothelial Dysfunction. *Cells* **2020**, *9* (7), 1652.

(20) Ordanini, S.; Varga, N.; Porkolab, V.; Thépaut, M.; Belvisi, L.; Bertaglia, A.; Palmioli, A.; Berzi, A.; Trabattoni, D.; Clerici, M.; et al. Designing Nanomolar Antagonists of DC-SIGN-Mediated HIV Infection: Ligand Presentation Using Molecular Rods. *Chem. Commun.* **2015**, *51* (18), 3816–3819.

(21) Chiodo, F. Temp-Ref-Novel ACE2-Independent Carbohydrate-Binding of SARS-CoV-2 Spike Protein to Host Lectins and Lung Microbiota.

(22) Thepaut, M.; Luczkowiak, J.; Vives, C.; Labiod, N.; Bally, I.; Lasala, F.; Grimoire, Y.; Fenel, D.; Sattin, S.; Thielens, N.; et al. DC/L-SIGN Recognition of Spike Glycoprotein Promotes SARS-CoV-2 Trans-Infection and Can Be Inhibited by a Glycomimetic Antagonist. *Biorxiv* **2020**, 2020.08.09.242917.

(23) Katz, D. H.; Tahir, U. A.; Ngo, D.; Benson, M. D.; Bick, A. G.; Pampana, A.; Gao, Y.;

Keyes, M. J.; Correa, A.; Sinha, S.; et al. Proteomic Profiling in Biracial Cohorts Implicates DC-SIGN as a Mediator of Genetic Risk in COVID-19. *Medrxiv* **2020**, 2020.06.09.20125690.

(24) Mazzon, M.; Marsh, M. Targeting Viral Entry as a Strategy for Broad-Spectrum Antivirals. *F1000Research* **2019**, *8*, 1628.

(25) Zakaria, M. K.; Carletti, T.; Marcello, A. Cellular Targets for the Treatment of Flavivirus Infections. *Front. Cell. Infect. Microbiol.* **2018**, *8*.

(26) Krishnan, M.; Garcia-Blanco, M. Targeting Host Factors to Treat West Nile and Dengue Viral Infections. *Viruses* **2014**, *6* (2), 683–708.

(27) Rodríguez-Pérez, L.; Ramos-Soriano, J.; Pérez-Sánchez, A.; Illescas, B. M.; Muñoz, A.; Luczkowiak, J.; Lasala, F.; Rojo, J.; Delgado, R.; Martín, N. Nanocarbon-Based Glycoconjugates as Multivalent Inhibitors of Ebola Virus Infection. *J. Am. Chem. Soc.* **2018**, *140* (31), 9891–9898.

(28) Ramos-Soriano, J.; Reina, J. J.; Illescas, B. M.; De La Cruz, N.; Rodríguez-Pérez, L.; Lasala, F.; Rojo, J.; Delgado, R.; Martín, N. Synthesis of Highly Efficient Multivalent Disaccharide/[60]Fullerene Nanoballs for Emergent Viruses. *J. Am. Chem. Soc.* **2019**, *141* (38), 15403–15412.

(29) Schwegmann, A.; Brombacher, F. Host-Directed Drug Targeting of Factors Hijacked by Pathogens. *Sci. Signal.* **2008**, *1* (29), re8–re8.

(30) Dam, T. K.; Brewer, C. F. Multivalent Lectin—Carbohydrate Interactions. In *Advances in carbohydrate chemistry and biochemistry*; 2010; Vol. 63, pp 139–164.

(31) Dam, T. K.; Gerken, T. A.; Cavada, B. S.; Nascimento, K. S.; Moura, T. R.; Brewer, C. F. Binding Studies of α-GalNAc-Specific Lectins to the α-GalNAc (Tn-Antigen) Form of Porcine Submaxillary Mucin and Its Smaller Fragments. *J. Biol. Chem.* **2007**, *282* (38), 28256–28263.

(32) Dam, T. K.; Brewer, C. F. Effects of Clustered Epitopes in Multivalent Ligand-Receptor Interactions. *Biochemistry* **2008**, *47* (33), 8470–8476.

(33) Lee, R. T.; Lee, Y. C. Affinity Enhancement by Multivalent Lectin-Carbohydrate Interaction. *Glycoconjugate Journal*. Springer 2000, pp 543–551.

(34) Becer, C. R.; Gibson, M. I.; Geng, J.; Ilyas, R.; Wallis, R.; Mitchell, D. A.; Haddleton, D. M. High-Affinity Glycopolymer Binding to Human DC-SIGN and Disruption of DC-SIGN Interactions with HIV Envelope Glycoprotein. *J. Am. Chem. Soc.* **2010**, *132* (43), 15130–15132.

(35) Ng, S.; Bennett, N. J.; Schulze, J.; Gao, N.; Rademacher, C.; Derda, R. Genetically-

Encoded Fragment-Based Discovery of Glycopeptide Ligands for DC-SIGN. *Bioorg. Med. Chem.* **2018**.

(36) Wang, S.-K.; Liang, P.-H.; Astronomo, R. D.; Hsu, T.-L.; Hsieh, S.-L.; Burton, D. R.; Wong, C.-H. Targeting the Carbohydrates on HIV-1: Interaction of Oligomannose Dendrons with Human Monoclonal Antibody 2G12 and DC-SIGN. *Proc. Natl. Acad. Sci. U. S. A.* **2008**, *105* (10), 3690–3695.

(37) Martínez-Ávila, O.; Bedoya, L. M.; Marradi, M.; Clavel, C.; Alcamí, J.; Penadés, S. Multivalent Manno-Glyconanoparticles Inhibit DC-SIGN-Mediated HIV-1 Trans-Infection of Human T Cells. *ChemBioChem* **2009**, *10* (11), 1806–1809.

(38) Taouai, M.; Porkolab, V.; Chakroun, K.; Cheneau, C.; Luczkowiak, J.; Abidi, R.; Lesur, D.; Cragg, P. J.; Halary, F.; Delgado, R.; et al. Unprecedented Thiacalixarene Fucoclusters as Strong Inhibitors of Ebola Cis-Cell Infection and HCMV-GB Glycoprotein/DC-SIGN C-Type Lectin Interaction. *Bioconjug. Chem.* **2019**, *30* (4), 1114–1126.

(39) Owen, K. Regulatory Toxicology Considerations for the Development of Inhaled Pharmaceuticals. *Drug Chem. Toxicol.* **2013**, *36* (1), 109–118.

(40) Lim, Y. H.; Tiemann, K. M.; Hunstad, D. A.; Elsabahy, M.; Wooley, K. L. Polymeric Nanoparticles in Development for Treatment of Pulmonary Infectious Diseases. *Wiley Interdiscip. Rev. Nanomedicine Nanobiotechnology* **2016**, *8* (6), 842–871.

(41) Rai, R.; Alwani, S.; Badea, I. Polymeric Nanoparticles in Gene Therapy: New Avenues of Design and Optimization for Delivery Applications. *Polymers (Basel).* **2019**, *11* (4), 745.

(42) Herrendorff, R.; Hänggi, P.; Pfister, H.; Yang, F.; Demeestere, D.; Hunziker, F.; Frey, S.; Schaeren-Wiemers, N.; Steck, A. J.; Ernst, B. Selective in Vivo Removal of Pathogenic Anti-MAG Autoantibodies, an Antigen-Specific Treatment Option for Anti-MAG Neuropathy. *Proc. Natl. Acad. Sci.* **2017**, *114* (18), E3689–E3698.

(43) Aliu, B.; Demeestere, D.; Seydoux, E.; Boucraut, J.; Delmont, E.; Brodovitch, A.; Oberholzer, T.; Attarian, S.; Théaudin, M.; Tsouni, P.; et al. Selective Inhibition of Anti-MAG IgM Autoantibody Binding to Myelin by an Antigen-Specific Glycopolymer. *J. Neurochem.* **2020**.

(44) Hoppe, C. A.; Lee, Y. C. Accumulation of a Nondegradable Mannose Ligand within Rabbit Alveolar Macrophages. Receptor Reutihzation Is Independent of Ligand Degradation. *Biochemistry* **1984**, *23* (8), 1723–1730.

(45) Thoma, G.; Patton, J. T.; Magnani, J. L.; Ernst, B.; Öhrlein, R.; Duthaler, R. O. Versatile

Functionalization of Polylysine: Synthesis, Characterization, and Use of Neoglycoconjugates. *J. Am. Chem. Soc.* **1999**, *121* (25), 5919–5929.

(46) Watanabe, Y.; Bowden, T. A.; Wilson, I. A.; Crispin, M. Exploitation of Glycosylation in Enveloped Virus Pathobiology. *Biochim. Biophys. Acta - Gen. Subj.* **2019**, *1863* (10), 1480–1497.

(47) Fehres, C. M.; Kalay, H.; Bruijns, S. C. M.; Musaafir, S. A. M.; Ambrosini, M.; Van Bloois, L.; Van Vliet, S. J.; Storm, G.; Garcia-Vallejo, J. J.; Van Kooyk, Y. Cross-Presentation through Langerin and DC-SIGN Targeting Requires Different Formulations of Glycan-Modified Antigens. *J. Control. Release* **2015**, *203*, 67–76.

(48) Cairo, C. W.; Gestwicki, J. E.; Kanai, M.; Kiessling, L. L. Control of Multivalent Interactions by Binding Epitope Density. *J. Am. Chem. Soc.* **2002**, *124* (8), 1615–1619.

(49) Gestwicki, J. E.; Cairo, C. W.; Strong, L. E.; Oetjen, K. A.; Kiessling, L. L. Influencing Receptor−Ligand Binding Mechanisms with Multivalent Ligand Architecture. *J. Am. Chem. Soc.* **2002**, *124* (50), 14922–14933.

(50) Ting, S. R. S.; Chen, G.; Stenzel, M. H. Synthesis of Glycopolymers and Their Multivalent Recognitions with Lectins. *Polym. Chem.* **2010**, *1* (9), 1392.

(51) Igde, S.; Röblitz, S.; Müller, A.; Kolbe, K.; Boden, S.; Fessele, C.; Lindhorst, T. K.; Weber, M.; Hartmann, L. Linear Precision Glycomacromolecules with Varying Interligand Spacing and Linker Functionalities Binding to Concanavalin A and the Bacterial Lectin FimH. *Macromol. Biosci.* **2017**, *17* (12), 1700198.

(52) Murray, C. W.; Verdonk, M. L. Entropic Consequences of Linking Ligands. In *Fragment-based Approaches in Drug Discovery*; Wiley Blackwell, 2006; Vol. 34, pp 55–66.

(53) Dam, T. K.; Brewer, C. F. Thermodynamic Studies of Lectin-Carbohydrate Interactions by Isothermal Titration Calorimetry. *Chem. Rev.* **2002**, *102* (2), 387–429.

(54) Jencks, W. P. On the Attribution and Additivity of Binding Energies. *Proc. Natl. Acad. Sci. U. S. A.* **1981**, *78* (7 I), 4046–4050.

(55) Zhou, H. X.; Gilson, M. K. Theory of Free Energy and Entropy in Noncovalent Binding. *Chem. Rev.* **2009**, *109* (9), 4092–4107.

(56) Scheuermann, T. H.; Brautigam, C. A. High-Precision, Automated Integration of Multiple Isothermal Titration Calorimetric Thermograms: New Features of NITPIC. *Methods* **2015**, *76*, 87–98.

(57) Brautigam, C. A.; Zhao, H.; Vargas, C.; Keller, S.; Schuck, P. Integration and Global Analysis of Isothermal Titration Calorimetry Data for Studying Macromolecular

Interactions. *Nat. Protoc.* **2016**, *11* (5), 882–894.

(58) Piszczek, G. SEDPHAT – A Platform for Global ITC Analysis and Global Multi-Method Analysis of Molecular Interactions. *Methods* **2015**, *76*, 137–148.

(59) Schuck, P. Size-Distribution Analysis of Macromolecules by Sedimentation Velocity Ultracentrifugation and Lamm Equation Modeling. *Biophys. J.* **2000**, *78* (3), 1606–1619.

(60) Laue, T. M.; Shah, B. D.; Ridgeway, T. M.; Pelletier, S. L. *Computer- Aided Interpretation of Analytical Sedimentation Data for Proteins*; Harding, S. E., Rowe, A. J., Horton, J. C., Eds.; The Royal Society of Chemistry: Cambridge, United Kingdom, 1992.

(61) Durchschlag, H.; Zipper, P. Calculation of the Partial Volume of Organic Compounds and Polymers. In *Progress in Colloid & Polymer Science*; Springer-Verlag GmbH & Company KG, 1994; Vol. 94, pp 20–39.

(62) Brautigam, C. A. Calculations and Publication-Quality Illustrations for Analytical Ultracentrifugation Data. *Methods Enzymol.* **2015**, *562*, 109–133.

(63) Brown, P. H.; Balbo, A.; Schuck, P. Characterizing Protein-Protein Interactions by Sedimentation Velocity Analytical Ultracentrifugation. *Curr. Protoc. Immunol.* **2008**, *81* (1), Unit 18.15.

(64) Wu, L.; Martin, T. D.; Carrington, M.; KewalRamani, V. N. Raji B Cells, Misidentified as THP-1 Cells, Stimulate DC-SIGN-Mediated HIV Transmission. *Virology* **2004**, *318* (1), 17–23.

(65) Binley, J. M.; Ngo-Abdalla, S.; Moore, P.; Bobardt, M.; Chatterji, U.; Gallay, P.; Burton, D. R.; Wilson, I. A.; Elder, J. H.; de Parseval, A. Inhibition of HIV Env Binding to Cellular Receptors by Monoclonal Antibody 2G12 as Probed by Fc-Tagged Gp120. *Retrovirology* **2006**, *3*, 39.